applied sciences

MDPI

Article

Theoretical Investigation of Laser Induced Magnetization Reversal by Spin Orbit Coupling and Stimulated Raman Scattering

Yuhao Zou [1], Haiwei Wang [1,*], Yao Xiao [1], Zhihao Zeng [1], Lanlan Huang [1], Kai Wang [2], Sicong Wang [3], Xiangping Li [3] and Changsheng Xie [1]

1 Wuhan National Laboratory of Optoelectronics, Huazhong University of Science and Technology, Wuhan 430074, China; yuhao_zou@hust.edu.cn (Y.Z.); m201672656@hust.edu.cn (Y.X.); mizhengzzh@hust.edu.cn (Z.Z.); huanglanlan@hust.edu.cn (L.H.); cs_xie@hust.edu.cn (C.X.)

2 School of Physics, Huazhong University of Science and Technology, Wuhan 430074, China; kale_wong@hust.edu.cn

3 Guangdong Provincial Key Laboratory of Optical Fiber Sensing and Communications, Institute of Photonics Technology, Jinan University, Guangzhou 510632, China; wangsc@jnu.edu.cn (S.W.); xiangpingli@jnu.edu.cn (X.L.)

* Correspondence: hiway@hust.edu.cn; Tel.: +86-135-1722-6968

Received: 19 November 2018; Accepted: 21 December 2018; Published: 29 December 2018

Abstract: We theoretically study the mechanism of the all-optical magnetic switching by combining the Rashba effect and stimulated Raman scattering. In hydrogenlike systems, we show that the Rashba effect splits the energy band and stimulated Raman scattering transits the electrons between the lambda three-level system and controls the spin states to reverse the orientation of magnetization. The dynamics of electrons are described with the Lindblad equation in a few hundreds of femtoseconds. We further investigate the influence of laser intensity and wavelength on the probability of spin-flip in a ferromagnetic material, CoPt.

Keywords: All-optical switching; Rabi model; Rashba effect

1. Introduction

It has been reported that circularly polarized femtosecond laser pulses can deterministically switch the orientations of magnetization of certain materials [1–5], including rare-earth transition metal alloys [3,6], CoPt [7–9], and their multilayer films [10]. However, the fundamental mechanism remains an open question that impedes the further development of study.

All-optical magnetic switching is phenomenologically explained as a combination of effects derived from the inverse Faraday effect (IFE) [11–13] and heat described as the two-temperature model [5,14–18], and all can be treated as effective magnetic fields [5,19–21]. However, in a microscopic scale, the origin of IFE and the interaction between laser pulses and magnetic materials is only studied in few publications [12,22]. The early attempt carried out by Pitaevskii et al. [11] in 1961 theoretically predicted the existence of IFE in the frame of a thermodynamic potential. The first experimental observation of IFE was published by Ziel et al. [13] in 1965; Pershan et al. [12] explained the origin of the IFE from the view of quantum mechanics, and gave a quantitative expression for the IFE field. However, the derived effective Hamiltonian and standard magnetic field by Pershan, $M_{(t)} \propto E_{(t)} * E^*_{(t)}$, is not applicable for sub-picosecond and high-intensity laser scenarios, because the research assumed that the variation of the pulse amplitude is negligible during the magnetization switching process. The two-temperature model is proposed to reconcile the contradiction between the time scale and the

magnitude of magnetic field [4]. However, heat alone can only demagnetize the magnetic materials [23], if the material is not an anti-ferromagnetic system.

To suitably fit the study for the process of ultra-fast magnetization reversal, IFE derived by stimulated Raman scattering (SRS) was proposed by Popova [24,25] who deduced the effective magnetic field from the second order of the time-dependent Hamiltonian. In her study, SRS stimulates the electron transition and changes the spin state, which is helicity dependent, in magnetic materials. Instead of the Schrodinger picture, we are going to use the density matrix formalism to describe the transitions which allows introducing the decay rate easily.

In recent studies, the Rashba effect [26–28] is engineered to be coupled to laser schemes [29–31]. The circularly polarized laser-induced Rashba effect produces an effective magnetic field on CoPt [31]. The effective field is opposite to the magnetization direction; however, the magnitude of the effective field is helicity dependent. For left-handed circularly polarized light and magnetization along the z direction that is normal to the sample, the effective field is much greater than the right-handed circularly polarized laser-induced effective field. During the oscillation of electronic dipole transition, the angular moment should obey conservation law, which forbids the transitions with spin flips. The effective field induced by the Rashba effect contributes to the angular moment injection of the three-level system during the transitions, besides the function of splitting the energy band.

According to Pitaevskii and Pershan et al., the inverse Faraday field consists of two processes: (1) the light is directly interacted with magnetic materials, and (2) this interaction produces a quasi-stationary relaxed state, which leads to the birth of magnetization in the sample. In this paper, SRS is discussed both qualitatively and quantitatively in the transient process, which corresponds to the direct interaction of light with materials. The Rashba effect, the sub-picosecond time scale process [32], is treated as the builder of the quasi-stationary state.

Here, we utilize the ab initio theorem with the two effects mentioned above to get the insight of transient process of magnetization switching on a femtosecond scale. The Rashba effect-induced fine structure is spin-dependent, so the sub-bands are exclusive for spin-up or spin-down. More importantly, the effective field supplies a tunnel to flip spins at an excited state. The laser drives electrons to oscillate between the two sub-bands and virtual excited state, and all of the three constitute a Λ three-level system. In these transitions, spin-up may transform to spin-down, and all the oscillation will be described in the Rabi model [33–35]. We specify the simulation on CoPt which is commonly investigated by previous studies [8,12,31]. The final probability of spin state is controllable with the intensity and wavelength of laser.

2. Interaction of Light and Medium

In consideration of the result of Qaiumzadeh et al. [31], the laser-induced Rashba effect is treated as an effective magnetic field. As shown in Figure 1, the sub-bands $|1>$ and $|3>$ split by the effective field and the virtual state $|2>$ constitute the Λ three-level system. For the femtosecond laser, the monochromaticity is relatively poor. ω_e and ω_r correspond to different wavelengths included in the femtosecond laser. Δ_e (Δ_r) is the mismatch of the energy of the incident photos, ω_e (ω_r), and the energy gap between $|1>$ and $|2>$, ω_{12} ($|3>$ and $|2>$, ω_{23}).

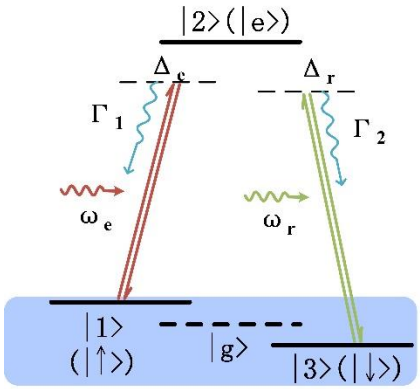

Figure 1. The schematic diagram of a Λ three-level system. The ground state is split into two fine energy bands, caused by the Rashba effect, in the ming blue background. |1> and |3> are spin-up or -down, respectively. |e> is a virtual state in the stimulated Raman scattering process, Γ_1 and Γ_2 are the decay rates.

The dynamics of electrons shown in Figure 1 describe the process of SRS [36,37]. Electrons are originally steady at state |1> with spin-up. After the incidence of laser, electrons are stimulated to virtual state |2>. Meanwhile, the incident laser, including the frequency ω_r that is approximate to ω_{23}, stimulates electrons radiating to state |3>. Therefore, SRS transfers electrons between different energy bands; the Rashba effect-induced effective field gives states |1> and |3> with specific spin states. More importantly, the effective field does not only maintain the quasi-stationary state, but also break the transition forbidden for spin-flip.

We are going to use the Rabi model to describe the process of SRS instead of the form of nonlinear polarization, because the distribution of laser in the spatial domain is neglected. However, in the framework of the Rabi model without decay, electrons will remain on the virtual state, because of the sudden stop of the laser. Therefore, we investigate the transition in a three-level system by the Lindblad equation, which is easy to describe how a density operator evolves in an open system with decay. Diagonal elements of the density matrix represent the probability of electrons occupying the state:

$$\dot{\rho} = -\mathrm{i}[H, \rho] + \mathrm{L}_{(\rho)} \tag{1}$$

$$\mathrm{L}_{(\rho)} = C\rho C^* - \frac{1}{2}(C^*C\rho + \rho C^*C) \tag{2}$$

where the first term of the right-hand side of Equation (1) is the Liouville-von Neumann equation [33], describing the unitary evolution of the density operator; ρ is the density matrix of the three-level system and $\dot{\rho}$ represents the elements of density matrix take a derivative of time; H is a 3 × 3 matrix expression of Hamiltonian and the elements of the matrix are written as ω_{nm}; C describes the decay of electrons to ground state; C^* is the transpose of C. We choose specific time-dependent phases to simplify the diagonal elements of H, and define the elements as:

$$\begin{gathered} W_{11} = 0,\ W_{22} = \hbar\Delta_1 = \hbar\Delta_e, \\ W_{33} = \hbar\Delta_2 = \hbar(\Delta_e - \Delta_r) \end{gathered} \tag{3}$$

$$\Delta_e = \omega_{12} - \omega_e,\ \Delta_r = \omega_{23} - \omega_r \tag{4}$$

where ω_{12} and ω_{23} are the angular frequencies corresponding to the difference of energy of states |2>, |1> and |2>, |3>, respectively; ω_e and ω_r are the angular frequencies of incident femtosecond laser.

The off-diagonal elements of interaction Hamiltonian is considered as electric dipole transitions, d_{nm}, for which an atomic dipole moment is affected by a classical electric field, $E_{nm}(t)$. $E_{nm}(t)$ is the

envelope of a Gaussian laser. Parameters followed by the subscript of nm represent that they are related with the interaction between states |n> and |m>.

$$W_{nm} = \frac{1}{2} d_{nm} \cdot E_{nm}(t), (n \neq m) \tag{5}$$

Therefore, the complete Hamiltonian is:

$$H = \begin{bmatrix} 0 & W_{12} & 0 \\ W_{12}^* & \Delta_1 & W_{23} \\ 0 & W_{23}^* & \Delta_2 \end{bmatrix} \tag{6}$$

For $L_{(\rho)}$, C is determined by decay rates γ_1 and γ_3:

$$C = \begin{bmatrix} 0 & \sqrt{\gamma_1} & 0 \\ 0 & 0 & 0 \\ 0 & \sqrt{\gamma_3} & 0 \end{bmatrix} \tag{7}$$

In the simulation, the time scale of incident laser is about 100 fs, which means the spectrum is extended. According to the uncertainty principle, $\Delta t \cdot \Delta \nu \geq 0.441$; for the Gaussian pulse, frequency bandwidth, $\Delta\nu$, is at least 4.4×10^{14} Hz. As shown in Figure 3a, it is possible that ω_{12} and ω_{23} are contained in one laser beam. ω_{12} and ω_{23} are defined by $\omega_{12} = \omega_0 - \Delta\omega$, and $\omega_{23} = \omega_0 + \Delta\omega$, respectively. ω_0 represents the energy difference between the initial ground state of material and the virtual state. $\Delta\omega$ is determined by the strength of the Rashba effect-induced effective field. $\Delta\omega = \alpha_R \cdot p$, where α_R is the Rashba coefficient and p is the momentum of electrons, which is tunable by adjusting the materials and structure. We choose the frequencies that $\omega_{23} = \omega_r$, and $\omega_{12} = \omega_e$ which is the most sensitive and predigests the computational complexity. The Rashba effect-induced band split, $2\Delta\omega$, may variate with the intensity of incident light, but the broad spectrum of femtosecond laser insures the self-adaption, maintaining $\omega_{23} = \omega_r$, and $\omega_{12} = \omega_e$. The Hamiltonian is evolved to:

$$H = \begin{bmatrix} 0 & W_{12} & 0 \\ W_{12}^* & 0 & W_{23} \\ 0 & W_{23}^* & 0 \end{bmatrix} \tag{8}$$

Substituting Equations (7) and (8) into Equations (1) and (2), the evolution of density matrix can be easily observed. The Hermitian Hamiltonian and Lindbladian terms guarantee the density matrix maintaining Hermitian in the duration of the laser interaction.

3. Discussion

3.1. Initial State of Material

Following the previous researches [7,25,31], we specify our investigation to ferromagnetic material CoPt, on which all-optical switching is dependent on the helicity of polarization. We attribute the helicity dependence to the Rashba effect-induced effective field [31] and the transition rules of SRS [25]. In the experiment, the material is pre-magnetized. However, considering the high intensity of laser, the temperature of electrons reaches the Curie temperature before the dramatic electron oscillations. Here, we briefly introduce the two-temperature model to demonstrate the ultrafast soar of electron temperature. The process is described by the two coupled equations:

$$\begin{aligned} C_e(T_e)\frac{dT_e}{dt} &= -G \cdot (T_e - T_p) + P, \\ \frac{dT_p}{dt} &= G \cdot (T_e - T_p)/C_p - (T_p - T_0) \cdot s \end{aligned} \tag{9}$$

where T_e and T_p represent the electron and phonon temperature, respectively; $C_e(T_e)$ and C_p are the specific heats of the electron and phonon, respectively; $C_e(T_e)$ is proportional to T_e, and $C_e(T_e) = C_0 \cdot T_e$; C_0 is the coefficient that does not relate to temperature; P is the pump power of the pulse, which follows the Gaussian distribution in intensity vs time. Additionally, we ignore the penetration loss for less than 20-nm-thickness thin films; G and s are the electron-phonon coupling constant and the heat sink coupling constant, respectively. The main parameters of the two-temperature model and the corresponding typical values are listed in our previous work [17].

The multilayer CoPt structure was firstly discovered the phenomenon of all-optical switching, but the Curie temperature, T_c, is not mentioned in the original paper [7]. We find that the Curie temperature is varied from the thickness of Co and Pt layers, but the Curie temperature is generally less than 500 K. [38,39] Figure 2 shows the temperature fluctuation of electrons and lattice in 1 ps. When electrons near the Curie temperature before the intensity of laser reaches highest, the magnetization disappears. Therefore, even though the magnetic material is pre-magnetized in the experiment, we initialize our simulation system with the balance state of spin-up and spin-down.

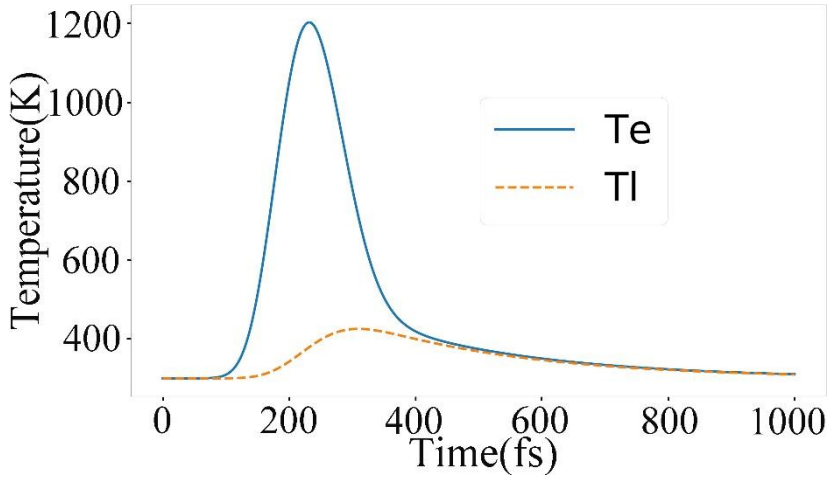

Figure 2. Two-temperature model for electrons and lattice. It can be seen that the temperature of electrons dramatically rises to T_c of 500 K from room temperature of 300K within 150 fs.

3.2. Spin State Transition

ω_0 is the intrinsic property of materials, but $\Delta\omega$ is determined by the intensity of laser. By controlling $\Delta\omega$ and the difference between the center frequencies of femtosecond laser ω and ω_0, the distributions of final spin states are various. Here, Figure 3a shows a specific relation between ω, ω_0 and $\Delta\omega$ ($\omega_{12} = \omega_0 - \Delta\omega$, $\omega_{23} = \omega_0 + \Delta\omega$) and the electric field of laser, $E_{12} = 2E_{23}$, where ω_{12} equals to the center frequency of the incident laser.

We ignore the difference of electric dipoles $d_{12} = d_{23}$, because $\Delta\omega$ is much less than ω_0; decay rates $\gamma_1 = \gamma_3 = 0.01$, which can be neglected during the interaction between laser and materials. The pick intensity of electric field, E_{12}, is ~10^9 V/m. The pulse width τ of the simulation in Figure 3 is 100 fs and the peak of the laser is reached at 2τ. In this model, the effective field induced by the Rashba effect breaks the transition forbidden with spin-flip, but the influence to the transition between |2> and |3> is not discussed. Instead, the magnitude of electric filed directly determines the speed of the transition.

Figure 3a shows the relationship between the incident laser and the energy gap of ω_{12} and ω_{23}. The full line describes the distribution of frequency versus the electric field. The intersections of vertical imaginary lines and the profile of the laser are corresponding to the magnitude of electric field for the interaction of laser and material. In Figure 3b, the intensity of electric dipole transition, ω_{12} and ω_{23} are 1.4 eV and 0.7 eV, respectively. ρ_1 and ρ_3 are the probabilities of spin state at |1> and |3>, respectively; initially, $\rho 1 = \rho 3 = 0.5$. The results in Figure 3b can be qualitatively explained by the fact that more electrons at state |1> are excited by higher intensity of laser than those at state

|3>, which maintains the population density at state |2>, while more electrons stimulated radiate to state |3>. The separate dynamics of the three states are ignored, but the process of magnetization is shown in Figure 3b, because the difference of the probability of spin-up and -down, $\Delta\rho = \rho_3 - \rho_1$, reflects the magnetization of the sample. The final state of $\Delta\rho$ is steady at about 0.11, which indicates a determinate all-optical magnetic switching.

Because of the equality of γ_1 and γ_3 which are assigned previously, electrons decay to |1> and |3> with the same speed. $\Delta\rho$ keeps constant after about 300 fs when there are electrons that remain staying at the virtual state. However, the decay rate should be considered with the surrounding areas. The direction of the magnetization of material after the interaction of laser affects the tendency to decaying to spin-up or -down. $\Delta\rho$ should be greater than the result displayed in Figure 3b, but we still assume that γ_1 equals to γ_3 in the following simulations, which does not significantly affect the final probability $\Delta\rho$.

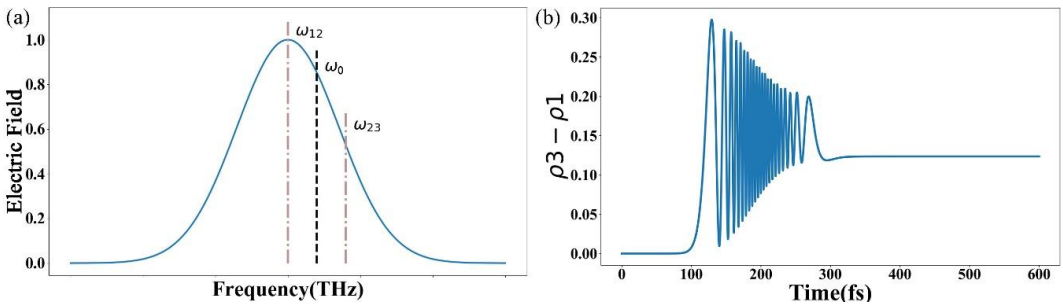

Figure 3. (**a**) The frequency spectrum of the femtosecond laser compared with the energy gap between |1> and |e> (ω_{12}), |g> and |e> (ω_0), |3> and |e> (ω_{23}). The intensity of electronic filed ω_{12} is twice that of ω_{23}. (**b**) Dependence of $\rho_3 - \rho_1$ on time. $\rho_3 - \rho_1$ represents the occupation probability difference between states |1> (spin-up) and |3> (spin-down). The spin determines the orientation of magnetization.

We further investigate the effect of the variation of the pulse width and the intensity of laser to the final state of $\Delta\rho$. In Figure 4, the intensity variation is reflected by ω_{12}. The summation of ω_{12} and ω_{23} is constant to be 2.1 eV and ω_{12} varies from 1.05 to 1.6 eV. τ represents the pulse width of laser; the peak of the intensity of laser is reached at 2τ; the simulation time is set as 6τ. $\Delta\rho$ oscillates when ω_{12} increases, but the tendency of $\Delta\rho$ is increased. The amplitude of the oscillation decreases with the augment of the pulse width τ. $\Delta\rho$ is approximately proportional to ω_{12} when the pulse width increases to 300 fs. Because of the short pulse width, the oscillation of electrons suddenly stops before the oscillation reaches equilibrium, whereas the envelop of the electric field with a long pulse width changes gradually so that electron oscillation can follow the variation of electric field. Therefore, the determination of the final spin state resulting from the duration of laser is not important when the pulse width is greater than 100 fs.

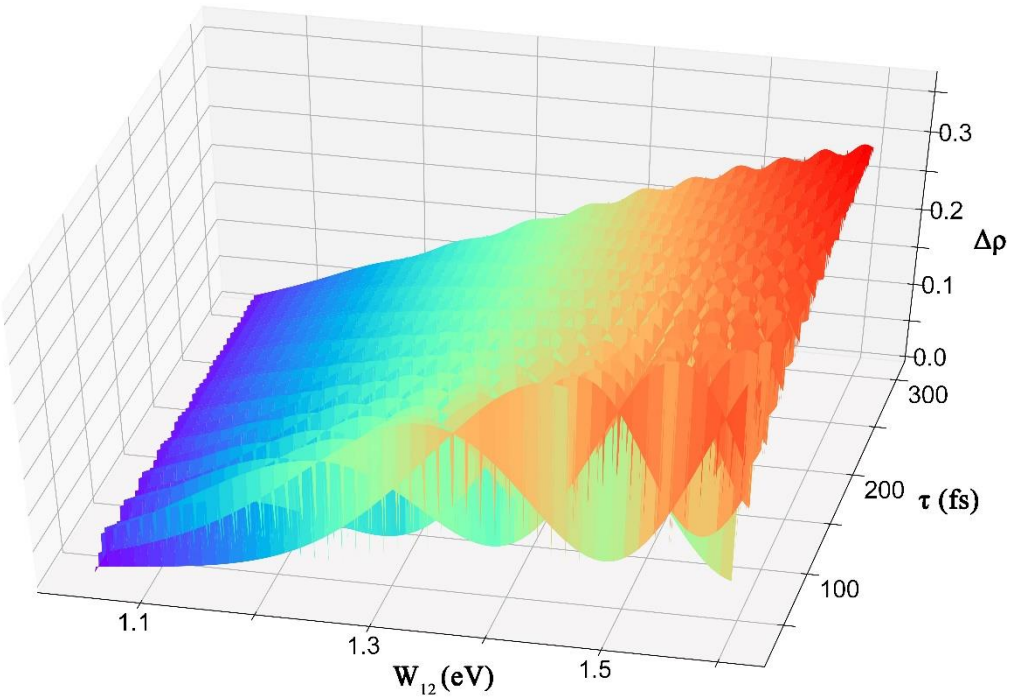

Figure 4. Δρ, the probability difference of states |3> and |1>, varies with ω_{12} and pulse width. When the pulse width is less than 100 fs and ω_{12} increases, Δρ increases with dramatic fluctuation. When the pulse width is larger than 100 fs, ω_{12} = 1.6, and ω_{23} = 0.5, Δρ approximately stabilizes at 0.28.

The wavelength and intensity-related spin-flip supplies a channel to control the final state of the magnetization. It is obvious that the spin states keep balanced when $E_{12} = E_{23}$ in Figure 4. When the sum of ω_{12} and ω_{23} is still 2.1 eV and ω_{12} decreases from 1.05 to 0.5 eV, Δρ will be odd symmetric to the flat of W12 = 1.05 in Figure 4. Therefore, by adjusting the distribution of the relative intensities that correspond to ω_{12} and ω_{23}, the area where the magnetization is reversed can be smaller than that of the incident laser.

4. Conclusions

All-optical magnetic switching is a sophisticated process that merges multi-effects influencing the spin state at different time scales and dominating at different times. We ignore the influence of magnetism and only investigate the first 6τ, when the interaction of laser and material preponderates. The heat breaks the initial state to the demagnetization and energy barrier for spin-flip. The Rashba effect splits the ground state to fine energy bands which are spin-dependent and keeps the angular moment conservation. SRS is treated as an adiabatic passage that transits electrons between spin-up and -down and the intermedia virtual excited state.

We utilize the framework of Rabi oscillation with the Lindblad equation to describe the process of electron transition and the dynamic of magnetization. The magnetization reflected by the difference of spin-up and -down is manipulated by the intensity of laser corresponding to a specific wavelength and a definite magnetization reversal is realized. After the pulse width is greater than 100 fs, the final state of the magnetization is approximately proportional to ω_{12}.

The model may be rough, but it reflects the dynamic of magnetization reversal. The discovery of the wavelength and intensity-sensitive magnetization reversal supplies a possible way to reduce the area of recorded size with the far field laser in the future. The next step of our investigation will focus on the combination of the process of SRS and traditional magnetism, because traditional magnetism supplies a complete theory to describe the dynamic of magnetization in a longer time scale.

Author Contributions: Y.Z. performed the simulation; H.W. edited and audited the content; C.X. acquired funding. All authors read and approved the manuscript.

Funding: This work is funded by the National Nature Science Foundation of China (NSFC) (grant No.: 61432007).

Conflicts of Interest: The authors declare no conflict of interest.

References

1. Kirilyuk, A.; Kimel, A.V.; Rasing, T. Ultrafast optical manipulation of magnetic order. *Rew. Mod. Phys.* **2010**, *82*, 2731. [CrossRef]
2. Stupakiewicz, A.; Szerenos, K.; Afanasiev, D.; Kirilyuk, A.; Kimel, A. Ultrafast nonthermal photo-magnetic recording in a transparent medium. *Nature* **2017**, *542*, 71–74. [CrossRef] [PubMed]
3. Stanciu, C.; Hansteen, F.; Kimel, A.; Kirilyuk, A.; Tsukamoto, A.; Itoh, A.; Rasing, T. All-optical magnetic recording with circularly polarized light. *Phys. Rev. Lett.* **2007**, *99*, 047601. [CrossRef] [PubMed]
4. Vahaplar, K.; Kalashnikova, A.; Kimel, A.; Hinzke, D.; Nowak, U.; Chantrell, R.; Tsukamoto, A.; Itoh, A.; Kirilyuk, A.; Rasing, T. Ultrafast path for optical magnetization reversal via a strongly nonequilibrium state. *Phys. Rev. Lett.* **2009**, *103*, 117201. [CrossRef] [PubMed]
5. Ostler, T.; Barker, J.; Evans, R.; Chantrell, R.; Atxitia, U.; Chubykalo-Fesenko, O.; El Moussaoui, S.; Le Guyader, L.; Mengotti, E.; Heyderman, L. Ultrafast heating as a sufficient stimulus for magnetization reversal in a ferrimagnet. *Nat. Commun.* **2012**, *3*, 666. [CrossRef] [PubMed]
6. Alebrand, S.; Gottwald, M.; Hehn, M.; Steil, D.; Cinchetti, M.; Lacour, D.; Fullerton, E.E.; Aeschlimann, M.; Mangin, S. Light-induced magnetization reversal of high-anisotropy TbCo alloy films. *Appl. Phys. A* **2012**, *101*, 162408. [CrossRef]
7. Lambert, C.-H.; Mangin, S.; Varaprasad, B.C.S.; Takahashi, Y.; Hehn, M.; Cinchetti, M.; Malinowski, G.; Hono, K.; Fainman, Y.; Aeschlimann, M. All-optical control of ferromagnetic thin films and nanostructures. *Science* **2014**, *345*, 1337–1340. [CrossRef] [PubMed]
8. Cornelissen, T.; Córdoba, R.; Koopmans, B. Microscopic model for all optical switching in ferromagnets. *Appl. Phys. Lett.* **2016**, *108*, 142405. [CrossRef]
9. Choi, G.-M.; Schleife, A.; Cahill, D.G. Optical-helicity-driven magnetization dynamics in metallic ferromagnets. *Nat. Commun.* **2017**, *8*, 15085. [CrossRef]
10. Mangin, S.; Gottwald, M.; Lambert, C.; Steil, D.; Uhlíř, V.; Pang, L.; Hehn, M.; Alebrand, S.; Cinchetti, M.; Malinowski, G. Engineered materials for all-optical helicity-dependent magnetic switching. *Nat. Mater.* **2014**, *13*, 286–292. [CrossRef]
11. Pitaevskii, L. Electric forces in a transparent dispersive medium. *Sov. Phys. JETP* **1961**, *12*, 1008–1013.
12. Pershan, P.; Van der Ziel, J.; Malmstrom, L. Theoretical discussion of the inverse Faraday effect, Raman scattering, and related phenomena. *Phys. Rev.* **1966**, *143*, 574. [CrossRef]
13. Van der Ziel, J.; Pershan, P.; Malmstrom, L. Optically-induced magnetization resulting from the inverse Faraday effect. *Phys. Rev. Lett.* **1965**, *15*, 190. [CrossRef]
14. Jiang, L.; Tsai, H.-L. Improved two-temperature model and its application in ultrashort laser heating of metal films. *J. Heat Transf.* **2005**, *127*, 1167–1173. [CrossRef]
15. Kimel, A.V.; Kirilyuk, A.; Rasing, T. Femtosecond opto-magnetism: Ultrafast laser manipulation of magnetic materials. *Laser Photon. Rev.* **2007**, *1*, 275–287. [CrossRef]
16. Huang, T.; Wang, H.; Zou, Y.; Cheng, W.; Xie, C. Explorations on size limit of L10-FePt nanoparticles for practical magnetic storage. *AIP Adv.* **2016**, *6*, 115302. [CrossRef]
17. Huang, T.; Wang, H.; Cheng, W.; Zou, Y.; Xie, C. Critical switching fluence of L10-FePt nanoparticles with practical size to ultrafast all-optical polarization switching. *EPL* **2017**, *118*, 67006. [CrossRef]
18. Steil, D.; Alebrand, S.; Hassdenteufel, A.; Cinchetti, M.; Aeschlimann, M. All-optical magnetization recording by tailoring optical excitation parameters. *Phys. Rev. B* **2011**, *84*, 224408. [CrossRef]
19. Evans, R.F.; Fan, W.J.; Chureemart, P.; Ostler, T.A.; Ellis, M.O.; Chantrell, R.W. Atomistic spin model simulations of magnetic nanomaterials. *J. Phys. Condens. Matter* **2014**, *26*, 103202. [CrossRef]
20. Evans, R.F.; Ostler, T.A.; Chantrell, R.W.; Radu, I.; Rasing, T. Ultrafast thermally induced magnetic switching in synthetic ferrimagnets. *Appl. Phys. Lett.* **2014**, *104*, 082410. [CrossRef]

21. Radu, I.; Vahaplar, K.; Stamm, C.; Kachel, T.; Pontius, N.; Dürr, H.; Ostler, T.; Barker, J.; Evans, R.; Chantrell, R. Transient ferromagnetic-like state mediating ultrafast reversal of antiferromagnetically coupled spins. *Nature* **2011**, *472*, 205–208. [CrossRef] [PubMed]
22. Battiato, M.; Barbalinardo, G.; Oppeneer, P.M. Quantum theory of the inverse Faraday effect. *Phys. Rev. B* **2014**, *89*, 014413. [CrossRef]
23. Atxitia, U.; Chubykalo-Fesenko, O.; Kazantseva, N.; Hinzke, D.; Nowak, U.; Chantrell, R.W. Micromagnetic modeling of laser-induced magnetization dynamics using the Landau-Lifshitz-Bloch equation. *Appl. Phys. A* **2007**, *91*, 232507. [CrossRef]
24. Popova, D. Microscopic description of the inverse Faraday effect at subpicosecond time scales. Available online: https://core.ac.uk/download/pdf/36614088.pdf (accessed on 20 December 2018).
25. Popova, D.; Bringer, A.; Blügel, S. Theoretical investigation of the inverse Faraday effect via a stimulated Raman scattering process. *Phys. Rev. B* **2012**, *85*, 094419. [CrossRef]
26. Manchon, A.; Koo, H.C.; Nitta, J.; Frolov, S.; Duine, R. New perspectives for Rashba spin-orbit coupling. *Nat. Mater.* **2015**, *14*, 871–882. [CrossRef] [PubMed]
27. Krupin, O.; Bihlmayer, G.; Starke, K.; Gorovikov, S.; Prieto, J.; Döbrich, K.; Blügel, S.; Kaindl, G. Rashba effect at magnetic metal surfaces. *Phys. Rew. B* **2005**, *71*, 201403. [CrossRef]
28. Miron, I.M.; Gaudin, G.; Auffret, S.; Rodmacq, B.; Schuhl, A.; Pizzini, S.; Vogel, J.; Gambardella, P. Current-driven spin torque induced by the Rashba effect in a ferromagnetic metal layer. *Nat. Mater.* **2010**, *9*, 230–234. [CrossRef] [PubMed]
29. Chen, X.-J. Fundamental mechanism for all-optical helicity-dependent switching of magnetization. *Sci. Rep.* **2017**, *7*, 41294. [CrossRef] [PubMed]
30. Edelstein, V.M. Inverse faraday effect in conducting crystals caused by a broken mirror symmetry. *Phys. Rev. Lett.* **1998**, *80*, 5766. [CrossRef]
31. Qaiumzadeh, A.; Titov, M. Theory of light-induced effective magnetic field in Rashba ferromagnets. *Phys. Rew. B* **2016**, *94*, 014425. [CrossRef]
32. Etienne, T.; Mosconi, E.; De Angelis, F. Dynamical Origin of the Rashba Effect in Organohalide Lead Perovskites: A Key to Suppressed Carrier Recombination in Perovskite Solar Cells? *J. Phys. Chem. Lett.* **2016**, *7*, 1638–1645. [CrossRef] [PubMed]
33. Shore, B.W. *Manipulating Quantum Structures Using Laser Pulses*; Cambridge University Press: Cambridge, UK, 2011.
34. Batista, A.A. Rabi oscillations in two-level systems beyond the rotating-wave approximation. *arXiv*, **2015**, arXiv:1507.05124.
35. Hughes, S. Breakdown of the area theorem: Carrier-wave Rabi flopping of femtosecond optical pulses. *Phys. Rev. Lett.* **1998**, *81*, 3363. [CrossRef]
36. Yang, X.; Wong, C.W. Coupled-mode theory for stimulated Raman scattering in high-Q/Vm silicon photonic band gap defect cavity lasers. *Opt. Express* **2007**, *15*, 4763–4780. [CrossRef] [PubMed]
37. Monfared, Y.E.; Ponomarenko, S.A. Non-Gaussian statistics of extreme events in stimulated Raman scattering: The role of coherent memory and source noise. *Phys. Rev. A* **2017**, *96*, 043817. [CrossRef]
38. Cai, W.; Muraishi, S.; Shi, J.; Nakamura, Y.; Liu, W.; Yu, R. Curie temperatures of CoPt ultrathin continuous films. *Appl. Phys. A* **2012**, *107*, 519–523. [CrossRef]
39. Inaba, N.; Igarashi, S.; Kirino, F.; Fujita, F.; Koike, K.; Kato, H. Magnetic properties of Co/Pt-Pd multilayer thin film media. *Phys. Status Solidi C* **2007**, *4*, 4498–4502. [CrossRef]